

## Superatom Chemistry: Promising Properties of Near-Spherical Noble Metal Clusters Perspective

Emil Roduner<sup>\*a,b</sup>

Properties of near-spherical metal clusters are best understood on the basis of the concept of conventional atoms. Their conduction electrons occupy cluster orbitals which remind of hydrogen-like orbitals since they have the same angular dependence. When populated with electrons, maxima in their ionization potentials and minima in electron affinities reveal the closing of shells in the same sense as for noble gases. This suggests that the periodic table of elements should be amended by a third dimension reflecting the number of atoms in a cluster of the element.

In a bonded situation the symmetry of cluster atoms is broken, and the atomic orbital momentum is quenched to a large extent. However, if superatoms are axially symmetric, there are superatomic orbital angular moments, which are locked along this symmetry axis. If their z-component is non-zero, this leads to large magnetic moments and to significant spin-orbit interactions, which greatly complicate spectroscopic observation. This magnetic interaction is anisotropic and may

lead to hysteresis loops with corresponding blocking temperatures up to room temperature. The number of unpaired electrons in such a system is crucial, and it may be influenced by doping with different atoms or by chemical bonds to capping ligands.

Stable superatom clusters with size-tuned, tailored band gaps and band edge energies may be attractive replacements of toxic or rare elements in photovoltaic cells or batteries. They furthermore form chemically inert and well-defined stoichiometric complexes with various ligands. This reminds of the established transition metal complexes and may lead to a novel branch of chemistry in which the central ion of organometallic complexes is replaced by a metal superatom.

### Introduction

Chemists have devised various concepts that describe properties of different classes of matter such as atoms, molecules, transition metal complexes, salts or metals. These concepts are communicated in specific languages with more or less fixed terminologies throughout the community of chemists. The terminologies are useful and convenient since they permit properties of each of these classes of matter to be explained with minimum effort. Metals and semiconductors are described by the concept of band structures which represent a high density of delocalised molecular orbital states. These extend over the entire specimen and either accommodate the valence electrons; alternatively they are partly filled or nearly empty and host the conduction electrons. But how should we describe a cluster of *e.g.* 13 Pt atoms? Is it a metal, a semiconductor, or should we rather call it a molecule? It will be shown here that its properties are often best understood using the concept of an atom.

Over the past three decades, the structures and properties of atomic and molecular clusters have raised considerable interest. In their attempt to bring systematics into the subject, Khanna and Jena coined the term *superatom* as follows: "Atomic clusters with suitable size and composition can be designed to mimic the chemistry of atoms in the Periodic Table. These clusters which can

be viewed as superatoms could then form the building blocks for a class of solids with unique structural, electronic, optical, magnetic, and thermodynamic properties."<sup>1,2</sup>

In order to mimic the properties of conventional atoms the valence electrons in superatoms must be delocalized over the entire cluster which must be atomically precise and near-spherical. Furthermore, the number of these electrons is crucial, as it is in ordinary atoms. Superatoms are therefore restricted to metallic elements, either single or alloyed. Although the conduction electrons in a semiconductor like silicon are also delocalized, the number of these is quite low and usually not exactly known, and clusters of semiconductors or even of insulators do not exhibit superatom properties.

Superatoms can be prepared in atomic beams and studied as free, bare clusters in vacuum. However, their practical application in chemistry is in the condensed phase, where they normally have to be protected from agglomeration and reaction with the environment. This can be done by embedding them in polymers, in the pores of zeolites, or more commonly, by capping their surface with adsorbed molecules. These capping agents can be innocent adsorbates, or they can affect the count of delocalized electrons by forming a chemical bond.

Khanna and Jena also suggested that the size of clusters of a given element could inspire chemists to construct a third dimension of the periodic table.<sup>1,2</sup> It is intriguing to add this 3<sup>rd</sup> dimension to the periodic table of Mendeleev who brought systematics into the 63

<sup>a</sup> Institute of Physical Chemistry, University of Stuttgart, D-70569 Stuttgart.

<sup>b</sup> Department of Chemistry, University of Pretoria, Pretoria, South Africa 0002

elements known in 1863 when he was 29 years old. The table was based on a periodicity in the chemical properties. Mendeleev claimed that he conceived it in a dream.<sup>3</sup> The fact that similar periodicities are found in clusters of identical atoms or of more than a single element may inspire to discover new chemistry by using superatoms as building blocks for novel materials. Philip Ball called the concept of superatoms 'a new kind of alchemy'.<sup>4</sup> Much of the early development of superatom chemistry was performed in collaboration by Castleman and Khanna.<sup>5</sup>

Clusters of noble gases and of closed-shell, small molecules are relatively straightforward to understand, but the situation becomes more complex when the clusters contain delocalized electrons and develop quantum-size behavior and properties reminding of metals or semiconductors. In particular, unusual magnetic properties have led to some confusion, although they are closely related to electronic structure. While it is not surprising that elements like Fe, Co, Ni and other elements which are ferromagnetic in the bulk lead to high-spin clusters it was unexpected at first that nanoparticles consisting of elements like Au, Pt or Pd which show no bulk ferromagnetism develop superparamagnetism, and the understanding is incomplete, the situation confusing and sometimes seemingly contradictory.<sup>6</sup> We believe that this is often due to insufficient characterization of the systems. For example, the number of member atoms in nanoparticles is not known precisely and therefore the number of unpaired electrons is also uncertain. Even for nanoclusters (a term that we use for a particle with an atomically precise or countable number of member atoms) the number of unpaired electrons may not be known because they are often protected by ligands which consume some of these unpaired electrons to form covalent bonds to the metal.

Further complications arise because of the effect of a magnetic field or the perturbation by a matrix or support on the energetic level structure. The simple jellium approximation and the related superatom model are a promising basis for an understanding of near-spherical clusters, but these models have not yet been used to the same extent as the principles of atomic physics of conventional atoms. In particular, the consequences of cluster orbital angular momentum has received little attention. It is the purpose of this Perspective to exploit this picture and its potential in relation to selected experimental data. Much of it will be based on platinum clusters and gold nanoparticles since some of the best-known systems that are not ferromagnetic in the bulk are based on these two noble elements.

## Fundamentals

### Spin and orbital angular moments

Before we dive into the properties of clusters, we remind of some basics of atomic physics. The main contributions to energy are due to the attractive Coulomb interaction of the charges of the electrons with the nucleus and the repulsive Coulomb interactions between the electrons. This interaction is reflected by the main quantum number  $n$ , and in the hydrogen atom all substates of  $n$  have the same energy. More subtle is the effect of angular momentum. It relates to a magnetic dipole moment. All atomic orbitals with an orbital quantum number  $\ell > 0$  possess an angular momentum that can be seen as the classical analog of a circular motion of a charge. Electrons have a spin  $s = 1/2$ , which also has the properties of angular momentum, but without a classical analog. Each moment is characterized by two quantum numbers, one for

the total moment ( $\ell$  and  $s$ ) and one for their z-components ( $|m_\ell| \leq \ell$  and  $m_s = \pm 1/2$ ). Angular moments are quantized vector properties, and their coupling follows the rules of vector addition. We use lower case symbols for the quantum numbers and for the moments of individual electrons and orbital moments, and the capital symbols encountered below stand for the for the total moments of a sum over unpaired electrons or of other moments in a system. Since angular moments possess a magnetic dipole moment they do not only couple with each other, they also interact with an external magnetic field by the Zeeman interaction. The interaction energy of an orbital moment with a magnetic field  $B$  equals  $m_\ell \mu_B B$ , where  $\mu_B$  is the Bohr magneton ( $9.274 \times 10^{-24} \text{ J T}^{-1}$  or  $5.788 \times 10^{-5} \text{ eV T}^{-1}$ ), for an electron spin it is  $m_s g_e \mu_B B$ , where  $g_e = 2.0023$  is the electron  $g$  factor. Furthermore, many nuclei have a nuclear spin, but the associated magnetic moment is much smaller than that of an electron, and it is therefore neglected in the present context.

The electronic states of isolated atoms are described by term symbols based on Hund's rules which relate (i) to the total spin angular momentum of unpaired electrons described by its quantum number  $S = \sum s_i$  and its spin multiplicity  $2S+1$  and (ii) to the orbital angular momentum represented by its quantum number  $L = \sum \ell_i$ . The two moments couple by  $LS$  coupling to a total angular momentum given by the quantum number  $J$ . Hund's first rule states that for a given electron configuration the term with maximum multiplicity (thus also maximum  $S$  or maximum number of unpaired electrons) has the lowest energy. The second rule states that for a given multiplicity the term with the largest value of  $L$  has the lowest energy. The third rule states that the ground state of an atom with a less than half-filled subshell is the one with the lowest value of  $J$ , for a more than half-filled subshell it is the one with the highest value of  $J$ . Also these total moments are characterized by two quantum numbers, one for the magnitude of the moments ( $S$ ,  $L$ , and  $J$ ) and one for their z-components ( $M_S$ ,  $M_L$ , and  $M_J$ ), where  $-S \leq M_S \leq +S$ , etc.

Hund's rules hold for isolated atoms in the absence of any significant perturbation, *i.e.* for spherical symmetry, and in the presence of the weak  $LS$  coupling (also called Russel-Saunders coupling) but not of the stronger spin-orbit ( $SO$ ) coupling. When the atom is chemically bound or embedded in a crystal that exerts a crystal field, the orbital angular momentum is often reduced or even absent and said to be "quenched". For example, in a methyl radical ( $\cdot\text{CH}_3$ ), which is planar, the unpaired electron occupies a p-orbital ( $p_x$ ,  $p_y$ , or  $p_z$ ).  $p_x$  and  $p_y$  are real orbitals and equivalent to linear combinations of the complex orbitals  $p_+$  ( $n = 0$ ,  $\ell = 1$ ,  $m_\ell = +1$ ) and  $p_-$  ( $n = 0$ ,  $\ell = 1$ ,  $m_\ell = -1$ ), but only the latter ones possess an angular momentum with non-zero z- component (Figure 1a). That the angular momentum is quenched manifests itself by the radical's  $g$ -value being close to the same as for the free electron,  $g_e = 2.0023$ . Deviations from  $g_e$  are due to  $SO$  coupling, and they can be both, positive or negative. Admixture of some orbital momentum comes in already if one of the atoms is *e.g.* chlorine (*i.e.* in  $\cdot\text{CH}_2\text{C}\ell$ ,  $g = 2.0066$ ).

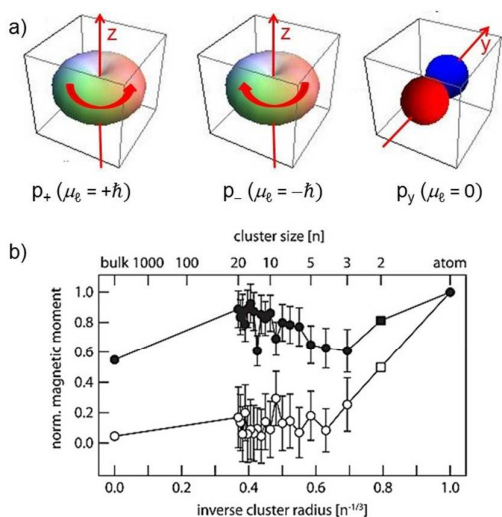


**Figure 1:** a) Complex hydrogen orbitals  $p_+$  ( $n = 0, \ell = 1, m_\ell = +1$ ) and  $p_-$  ( $n = 0, \ell = 1, m_\ell = -1$ ) and the real orbital  $p_y$  ( $n = 0, \ell = 1, m_\ell = 0$ ) that is a linear combination of  $p_+$  and  $p_-$ . The orbital momentum of the wave functions is  $m_\ell \hbar$ , thus it is quenched for  $p_x$  and  $p_y$  but  $\pm 1$  for  $p_+$  and  $p_-$ . b) Spin (closed circles) and orbital (open circles) magnetic moments of  $\text{Fe}_n^+$  clusters, normalized by the corresponding values in the atom,  $\mu_S = 4 \mu_B$  and  $\mu_\ell = 2 \mu_B$ . The orbital moments are much more reduced than the spin moments, and they both reach approximately the value in the bulk already for the triatomic ion (Reprinted with permission from Ref. 9. Copyright (2012) by the American Physical Society).

Gold has an electron configuration  $[\text{Xe}]4f^{14}5d^{10}6s^1$ , which gives a doublet ground state (term symbol  $^2S_{1/2}$ ) with orbital angular momentum zero in the atom. In bulk gold, however, the ratio of spin and orbital magnetic moments is  $\mu_\ell/\mu_S = 0.28(4)$  as determined by X-ray magnetic circular dichroism (XMCD), which means that the electron occupies no longer a pure  $s$  state, and 22% of the magnetization is due to an atomic orbital moment.<sup>7</sup> Platinum has the configuration  $[\text{Xe}]4f^{14}5d^96s^1$ , giving a triplet atomic ground state (term symbol  $^3D_3$ ) with an orbital angular momentum of 2 and  $\mu_\ell/\mu_S = 2$ . In bulk platinum foil, much of this orbital momentum is quenched, giving  $\mu_\ell/\mu_S = 0.38(2)$ .<sup>8</sup>

In agreement with the above, XMCD measurements of spin and orbital moments of size-selected free iron cluster ions  $\text{Fe}_n^+$  ( $n = 3-20$ ) revealed that even in clusters as small as  $\text{Fe}_3^+$  the atomic orbital angular momentum is strongly quenched and reduced to 5-25% of its value in the free atom, while the spin angular momentum remains at 60-90% (Figure 1b).<sup>9</sup> This confirms that the formation of bonds quenches atomic orbital angular moments. Only in  $\text{Fe}_2^+$  the projection of the orbital angular momentum onto the molecular axis remains a good quantum number because of its cylindrical symmetry, resulting in the predicted orbital moment of  $1 \mu_B$  per atom. The quenching of the orbital angular moments is illustrated in Figure 2b.

The distinction between atomic and cluster orbital moments and their contribution to magnetic properties will be important for an understanding of Au and Pt based superatoms. The orientation of the superatom orbital moment  $\mu_L$  is illustrated in Figure 2c for a  $\text{Pt}_{13}$  cluster that is discussed further below.

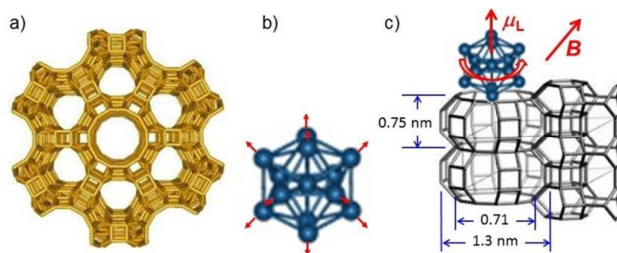


**Figure 2:** a) Structure of zeolite L viewed along the one-dimensional pores which host the 13-atom Pt clusters discussed in this work. b)  $\text{Pt}_{13}$  cluster. Arrows indicate the residual atomic orbital moments for which for symmetry reasons all components except the one perpendicular to the surface cancel out. These are the orbital moments measured by XMCD. c) Fragment of zeolite L structure with pore dimensions indicated and  $\text{Pt}_{13}$  cluster hosted by the pore (approximately to scale). The cylindrical symmetry of the pore determines the orientation of the superatom (cluster) orbital moment  $\mu_L$  that is locked to the environment and difficult to align in an applied magnetic field  $B$ .  $\mu_L$  is not accessible via XMCD.

We do not normally talk about chirality of free atoms. Nevertheless, orbitals like  $p_+$  and  $p_-$  shown in Figure 1a are mirror images due to their opposite helicity determined by the angular momentum. Since they are energetically degenerate any linear combination of them, like  $p_y$  with quenched angular momentum in the same figure, are equivalent solutions of the Schrödinger equation, and it is meaningless to talk about chirality. However, many superatom clusters are chiral, either imposed by the chirality of capping ligands, or even intrinsic with non-chiral ligands. Like chiral molecules, they cannot switch their chirality without breaking bonds and changing their structure to which the orientation of the orbital moment  $\mu_L$  has a fixed orientation analogous to the non-chiral case shown in Figure 2c, but with lower symmetry. While a large number of chiral gold clusters is chiral, mostly induced by their capping agents, the consequences have not yet been explored.<sup>10</sup>

### The electronic structure of superatoms: the jellium model

Much insight into the structure-stability behavior of clusters has come from atomic and molecular beams in which a high abundance of a certain mass is taken as evidence of extra stability of the corresponding cluster.<sup>11</sup> Numbers of members of particularly stable clusters were found to be often the same; they are therefore called *magic numbers*. For beams of clusters made of argon or of other noble gas atoms or indeed many molecular clusters which are held together by dispersion forces the highly abundant clusters correspond to 1, 13, 55, 147, 309, 561, 923, ... members, which is compatible with *geometrically closed shells* of icosahedral or cuboctahedral symmetry. A cluster of 13 members has one atom at the center and 12 nearest neighbors in direct contact with the central atom. An additional full shell can accommodate 42 atoms, leading to a total number of 55 members, etc. The high stability is due to the high coordination number of 6-9 and corresponding high cohesive energy for surface atoms in closed shells, compared with only 3 for the first adatom on the surface of the closed shell.

In contrast, it is found that sodium and other metals possess magic numbers of 2, 8, 20, 40, 58, 92, 138, 156, .... These are all even numbers, and it was concluded that they correspond to *electronically closed shells* with doubly occupied electronic states.

This is in full analogy to the electron configurations of noble gases, but with partly different quantum states,  $1s^2$  (electron count  $n = 2$ ),  $1s^2 1p^6$  ( $n = 8$ ),  $1s^2 1p^6 1d^{10} 2s^2$  ( $n = 20$ ), etc.<sup>12,13</sup> In metallic clusters, the valence electrons are treated as an electron gas in a continuous phenomenological potential box of square-well, parabolic or rounded square radial dependence that represents the attractive Coulomb potential of the not explicitly treated positive cores of all the cluster members (Figure 3a).<sup>12</sup> This is also called the *Jellium model*.

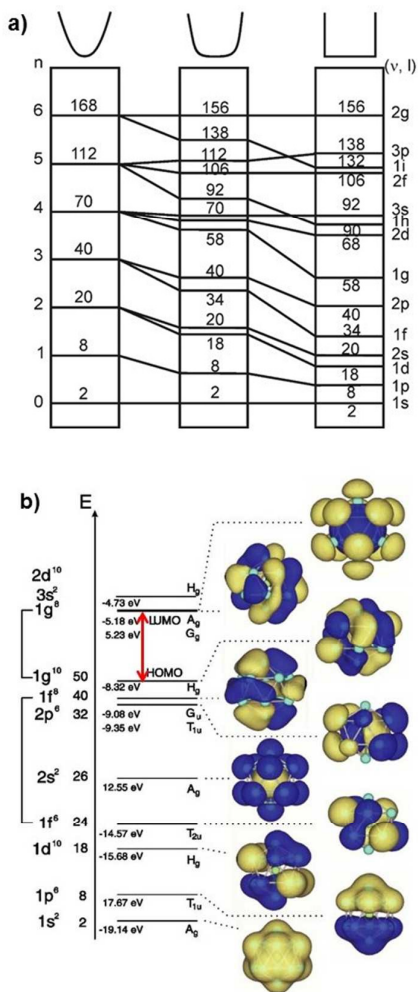


**Figure 3:** a) Single-electron energy levels for phenomenological quantum well potentials of parabolic, rounded square and purely square-well shapes with electron occupancy integrated from  $n = 0$  (Reprinted with permission from Ref. 12. Copyright (1993) by the American Physical Society). b) Calculated electronic orbitals (one for each set) for the core-shell icosahedral cluster  $AlPb_{12}^+$ . The overall cluster molecular orbitals resemble the spherical harmonics of atomic orbitals. On this ground, small clusters are often called 'superatoms' or 'pseudoatoms'. (Reprinted with permission from Ref. 14. Copyright (2004) by the American Physical Society).

We see that the energy and the degeneracy of the eigenstates depends significantly on the radial dependence of the centrally symmetric potential (Figure 3a). The phenomenological model can

be extended by using step functions for the potential with either a minimum or a maximum in the center to describe doped core-shell structures with either a more electronegative or more electropositive core. s-type wave functions which have a larger electron density in the center shift to lower energies in the first and to higher energies in the latter case.<sup>15</sup>

Figure 3b shows the result of DFT cluster molecular orbitals of the valence electrons of the icosahedral  $AlPb_{12}^+$  core-shell cluster ion. They are more accurate than those assumed in the Jellium model. With 4 electrons for each Pb and 3 for Al the cation has 50 electrons. This leads to a noble-gas-like closed-shell electronic system with all states filled up to the 5.23 eV HOMO-LUMO gap. Because of the closed-shell nature there is no distortion by the Jahn-Teller effect. The figure shows impressively that the molecular orbitals resemble those of atoms, with one nodal plane for p, two for d and three for f orbitals, and with one spherical nodal surface for 2s and two for 3s states. These cluster molecular orbitals, even though they are a bit dented because of the incorporated cores, are typical representatives of superatom orbitals as they are used here.

One other thing to note from Figure 3 is that the superatom orbital angular momentum quantum number increases in increments of 1, not limited by the restriction  $\ell \leq n-1$ , where  $n$  is the principal quantum number. This difference to the wave functions of the hydrogen atom originates in the shape of the radial potential, which is no longer a  $1/r$  Coulomb potential but a square well or a more complex shape. For example, for  $n = 1$  we have the singly degenerate s state, the triply degenerate p states, the five-fold degenerate d states, and the f-states corresponding to  $\ell = 3$  lead to seven-fold ( $2\ell + 1$ ) degenerate states which can host 14 electrons, g states ( $\ell = 4$ ) lead to nine-fold degenerate states. This holds for full spherical symmetry. However, the symmetry of the  $AlPb_{12}^+$  cluster is reduced to an icosahedron, which has a maximum degeneracy of five. Therefore, the 7 f states split into two groups of 3 and 4 degenerate orbitals, and the 9 g states into 5 and 4.

Thus we have two stability criteria for clusters, the geometric shell closing and the electronic shell closing. It is readily imagined that particular stability would arise if both principles were satisfied simultaneously. This can indeed be achieved, for example in  $Al_{13}^-$ . 13 atoms are compatible with a filled geometric shell around a central atom in both, icosahedral and cuboctahedral symmetry. Each Al atom contributes three valence electrons, so that the  $Al_{13}^-$  anion has 40 electrons, which is a closed shell for all three shapes of potential in Figure 3a. From the periodic table we are familiar with the octet rule, given by filled s and p shells. We furthermore have the powerful 18 electron rule for transition metals when the d-shell is filled in addition to s and p. We also have the stability rule of aromaticity, with  $4n + 2$  ( $n = 0, 1, 2, 3, \dots$ )  $\pi$  electrons.

Accepting the superatom nature of the cluster orbitals derived from atomic valence orbitals, we can take advantage of what we have learnt from the structure and symmetry of atomic orbitals. The analogy derives from the spherical symmetry of the system that leads to the identical spherical harmonic part of their wave functions, although the radial function is different. In particular, we expect the following features to hold:

- s-Orbitals have a finite amplitude at the center, all the others have a node. This contributes to the distinction between core and shell in core-shell nanoclusters.
- In addition to the electron's spin angular momentum and its atomic orbital momentum there is a superatomic orbital angular momentum.
- The influence of atomic orbital moments is limited due to the broken symmetry in bonded situations. However, the symmetry of near-spherical superatoms is high, allowing large superatomic orbital moments, which give rise to superatomic spin-orbit coupling. The consequence of this coupling has so far largely been neglected.<sup>16</sup> In the presence of *SO*-coupling, *S* and *L* are not good quantum numbers anymore, and an analog of Hund's rules is of limited value for superatoms.
- Orbital moments require the presence of cylindrical symmetry. Quantum mechanically, the magnetic moment undergoes precession about this axis. The classical analog is its z-component along this axis, called the "easy axis". Transverse components of the magnetization cancel, and oblate objects with degenerate in-plane easy axes have no net magnetic moment. Electrons in s-type orbitals (*L* = 0) have no orbital moment, and electrons in orbitals with *L* ≠ 0 but *L*<sub>z</sub> = 0 have also no net moment.
- Electric dipole allowed excitations of superatoms must be governed by selection rules just as for normal atoms, e.g. only transitions in which the superatomic orbital momentum changes by unity are allowed. Of course, perturbations of the symmetry by a matrix or due to the Jahn-Teller effect in open-shell systems will limit the rigidity of such selection rules.
- Compared to conventional atoms, the excitation of electronic transitions in superatoms can occur at much lower energies because of the higher density of states.
- There will be noble-gas-like closed-shell configurations which have no net spin and no net orbital moments. These may be highly degenerate because of the absence of spin-orbit coupling, and as a consequence there may be a comparatively large HOMO-LUMO gap that is indicative of concomitant extra stability of the system.
- Open-shell systems contain unpaired electrons in the highest orbitals. They are likely involved in binding the protective ligands. The number of electrons that remain unpaired is reflected in the magnetic properties, which therefore become dependent on the type and number of bound ligands. The simplest possible ligands are hydrogen atoms which can form a hydride type protecting shell, and it may be possible to actually "titrate" the unpaired electrons by adding more and more hydrogen. This will of course show up in the magnetic properties.

### A third dimension of the periodic table

Figure 3 suggests that we can fill electrons into our superatom orbitals in the same way as we fill our conventional atomic orbitals as we increase the atomic number along the periodic table. This inspires us to represent metal clusters of increasing member number or size and therefore valence electrons as a new periodic table that is shown in Figure 4 for gold clusters with up to 36 electrons. Each atom is considered to contribute one 6s valence electron to the superatom. Au<sub>2</sub>, Au<sub>8</sub>, Au<sub>20</sub>, Au<sub>34</sub>, are noble-gas-like, closed-shell configurations analogous to those of He, Ne, Ar, and Kr. This novel third dimension of the periodic table as a function of increasing number of cluster atoms of a single element is inspiring,

but it must be emphasized that this extension works only for metals, comprising nearly 80% of the known elements, and it requires that the correct number of valence electrons is taken into account. Some experimental and theoretical evidence for their shell structure is given further below.

The picture of superatoms developed so far is greatly complicated by the fact that clusters are thermodynamically unstable with respect to the corresponding bulk state. This does not matter for cluster beams in vacuum, but in liquid environments where they can encounter and sinter they are normally synthesized with a protecting shell of ligands or in the pores of zeolites. The ligands change the surface energy of the cluster and may therefore affect its structure.

The figure shows two periodic tables side-by-side. The top table is the standard periodic table for elements up to atomic number 36, with color coding: s-block (blue), d-block (yellow), and f-block (pink). The bottom table is a periodic table for gold clusters, with columns labeled Au<sub>1</sub> through Au<sub>36</sub> and rows labeled with their valence electron configurations (e.g., 1s<sup>1</sup>, 1s<sup>2</sup>, 1s<sup>2</sup>1p<sup>1</sup>, etc.). The color coding in the bottom table follows the same scheme as the top table.

**Figure 4:** Conventional periodic table of elements up to the atomic number 36 (upper entry) and periodic table of gold cluster superatoms up to Au<sub>36</sub>. Colour code: s progressions (blue), p (green), d (yellow), and f (pink); (adapted from Ref. 17).

More importantly, many of these ligands form covalent bonds to the cluster, for example in thiol-protected gold or hydrogen-passivated platinum clusters. This bond consumes previous conduction electrons of the metal core and changes the effective electron count in the delocalized system that is to be described by the superatom model. Häkkinen described the situation in detail for gold clusters.<sup>18</sup> He developed the so-called *unifying superatom concept* that describes all known thiolate, phosphine-halide or phosphine-thiolate protected *n*-atomic gold clusters of overall charge *q*, represented by a formula (L<sub>s</sub>-Au<sub>n</sub>X<sub>m</sub>)<sup>q</sup>, where L<sub>s</sub> represents *s* weak ligands such as phosphines that do not affect the delocalized electron count, and X<sub>m</sub> stands for electron-withdrawing ligands (halides or thiolates). Taking into account that gold contributes only its 6s electron, represented by *v* = 1, the number of electrons *n*\* of a stable closed delocalized electron shell is then given by *n*\* = *nv* – *m* – *q*. For example, a compound Au<sub>39</sub>Ce<sub>6</sub>(PH<sub>3</sub>)<sub>14</sub><sup>-</sup> has *n*\* = 39 · 1 – 6 + 1 = 34, since the *s* = 14 phosphine ligands are weak and inactive.<sup>18</sup> This corresponds to a closed-shell superatom electron configuration 1s<sup>2</sup>1p<sup>6</sup>1d<sup>10</sup>2s<sup>2</sup>1f<sup>14</sup> in the complex (compare Figure 3 for the notation), which agrees with the photoelectron spectroscopic observation of the anion of the free Au<sub>34</sub> cluster in the gas phase.<sup>18</sup>

While the above example applies for a closed-shell electron configuration, the observed superparamagnetic properties of gold and other clusters reveals that there are also open-shell clusters with sometimes large high-spin electron configurations. In fact, the magnetization of platinum clusters in zeolites can be tuned by the extent of hydrogen chemisorption.<sup>19</sup>

### Evidence from electronic properties

### The shell structure of metal clusters

The first ionization potentials and the electron affinity of elements as a function of increasing atomic number  $Z$  shows a well-known periodicity that is understood based on the shell structure of atoms (Figure 5a). It is most obvious for the first ionization potentials (IP) which adopt maximum values for the closed shells of noble gases while the first electron in the next shell is far more easily to remove. The electron affinities (EA) are of maximum magnitude when addition of an electron leads to completion of a shell. Comparison of EA of metal nanoclusters as a function of size reveals analogous progressions which correspond to completion of the superatomic shells of an electron gas in a potential box of Figure 3a and to noble-gas-like clusters with 2, 8, 20 and 34 member atoms in the periodic table shown in Figure 4. Experimental values and also the results of a shell model calculation are given in Figure 5b for gold nanoclusters up to 72 member atoms and available also for silver and copper clusters.<sup>20</sup> A pronounced odd-even effect due to population of each orbital with two electrons is seen for the lower shells, but for  $N > 34$  and  $N > 58$  the structure is more continuous as seen also in Figure 5a for the transition metals and rare earth elements.

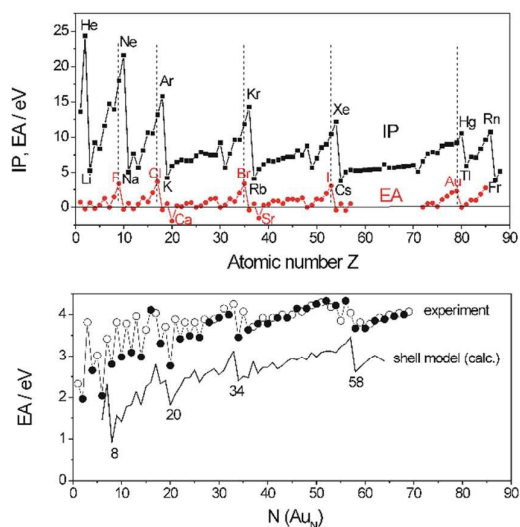


**Figure 5:** a) Ionisation potentials (IP) and electron affinities (EA) of elements in comparison with measured (circles) and b) on the basis of a shell model calculated (line) vertical electron affinities of  $Au_{1-70}$  as a function of cluster size. Even numbered cluster sizes are marked with a full dot. a) reproduced with permission from Ref. 17. b) reproduced with permission from Ref. 20 (Copyright (1992) American Institute of Physics).

The shell structure in Figure 5b is superimposed on a trend of the EA increasing with cluster size. EA evolves from 2.3 eV in the atom to 5.1 eV in the bulk metal. Simultaneously, IP evolves from 9.2 eV in the atom to the same 5.1 eV in the bulk, where the coinciding EA and IP are called *work function* (Figure 6). This size tuning is observed for all metals, and it is the most important size-effect in chemistry, and fundamental in particular in catalysis. It means that the availability to accept or donate electrons in oxidation or reduction reaction steps and in the effectiveness of forming covalent chemical bonds can be tuned by several eV, which is huge

compared with thermal energy of 26 meV at 300 K.<sup>17</sup> The closing of the HOMO-LUMO band gap with the size of small colloidal Au clusters embedded in dendrimeric poly(amidoamine) can be verified also from their fluorescence emission maxima, which are observed at 385 nm (3.22 eV) for  $Au_5$ , 455 nm (2.73 eV) for  $Au_8$ , 510 nm (2.43 eV) for  $Au_{13}$ , 760 nm (1.63 eV) for  $Au_{23}$ , and 866 nm (1.43 eV) for  $Au_{31}$ .<sup>21</sup> The structure of these embedded clusters is not known; small gold clusters in vacuum tend to be planar due to relativistic effects.<sup>18</sup>

A gold cluster of 72 atoms in Figure 5b is still sufficiently small to be non-metallic and display discrete molecular-like energy levels which allow for exciton formation. The transition regime to the metallic state starts at 144 atoms (4 shells, 1.7 nm diameter), and the metallic state that permits the excitation of collective electron motions and thus the formation of surface plasmon resonances starts at a size of 333 atoms (larger than 2.3 nm).<sup>22</sup>

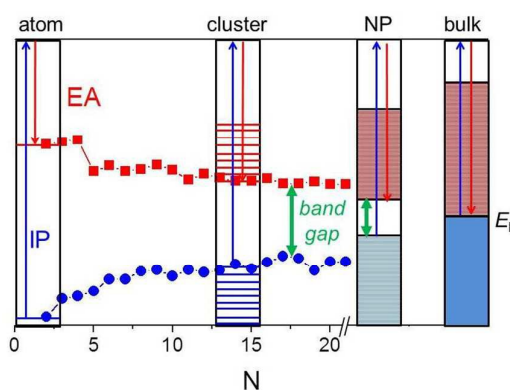


**Figure 6:** Schematic development of atomic energy level structure via clusters and semiconducting nanoparticles (NP) to bulk band structure. EA and IP change by several eV until they coincide in the bulk with the value of the Fermi energy  $|E_F|$ . This size-tuning is the most important size-effect of metal clusters in catalysis.

### Spin-orbit coupling in superatoms

**a) Gold:** The calculated splitting of the  $\ell = 2$ ,  $j = 3/2$  and  $j = 5/2$  states of atomic Pt and Au due to spin-orbit (SO) coupling has been reported to amount to  $5/2 \cdot \xi_d = 1.0$  eV and 1.06 eV, respectively.<sup>23</sup> It is more difficult to find unambiguous values for SO coupling of nanoclusters. However, data are available for a thiol-capped  $Au_{25}(SR)_{18}^-$  gold nanocluster that actually consists of a 13-atom icosahedral core containing 8 delocalized valence electrons. It is thus a species with closed geometric shell (magic number 13) and with 8 electrons also a closed electronic shell, which means double stabilization. The ligand shell consists of six dimeric RS–Au–SR–Au–SR motifs which contain the remaining gold atoms and consume the remaining 18 of the 26 gold valence electrons. The 13-atom core thus represents a closed-shell superatom with both, geometrical magic number 13 and electronic magic number 8. The optical spectrum shows splitting by 0.20 eV of a transition within the p manifold that should be unsplit in the absence of SO coupling (Figure 7). The splitting was confirmed convincingly to be due to SO coupling of the  $j = 1/2$  and  $j = 3/2$  p states in two-component DFT calculations.<sup>16</sup> It is considerably smaller than the 1.06 eV in atomic Au and of the order of the average level spacing

at the Fermi level that scales with the inverse volume and is expected to be *ca.* 1.50 eV / 13 = 0.11 eV for 13 Au atoms.<sup>24</sup>

The energy of the transition was calculated to be in the near infrared instead of the experimentally observed value of 1.8 eV (700 nm). This represents an offset by *ca.* 0.4 eV, which is ascribed to a known deficiency of the functional used in the calculation.<sup>16</sup> 1.8 eV is quite a large HOMO-LUMO gap as expected for closed-shell electron configurations of clusters of this size, indicating their pronounced stability.

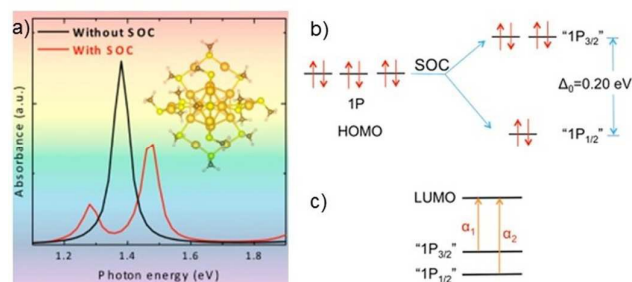


**Figure 7:** a) Structure and calculated optical transition of thiol-capped Au<sub>25</sub>(SR)<sub>18</sub><sup>-</sup> gold nanocluster, b) splitting of the triply degenerate superatomic 1p orbital due to *SO* coupling, and c) its effect on the optical absorption (reprinted with permission from Ref. 16. Copyright (2014) American Chemical Society).

**b) Platinum:** Information on the effect of *SO* coupling in superatoms is available also from density functional calculations for Pd<sub>13</sub> and Pt<sub>13</sub> nanoclusters of cuboctahedral and icosahedral symmetry.<sup>25,26</sup> Figure 8a shows the results of these calculations for 35 orbitals around the HOMO-LUMO gap with the 48 highest valence electrons of neutral icosahedral Pt<sub>13</sub>. The maximum degeneracy of icosahedral symmetry is five, as for the AlPb<sub>12</sub><sup>+</sup> cluster of Figure 3. However, this degeneracy comes to play only for closed-shell configurations. Figure 8a shows a high-spin state with six unpaired electrons. High-spin states are possible when the orbitals are within the spin pairing energy, which was reported to be on the order of 0.3 eV or less.<sup>27</sup> By comparison, the atomic orbitals of transition metal ions are more compact, and therefore the spin pairing energy amounts to typically about 1 eV.<sup>28</sup>

Open shell configurations lead to Jahn-Teller distortion of the symmetry. More importantly, unpaired electron spins in orbitals with non-zero angular momentum undergo *SO*-interaction. In Pt<sub>13</sub> clusters,  $\xi$  is of the order of 0.6 eV, and this affects the energies of cluster orbitals by up to 2.5 eV for high angular moments, which is two orders of magnitude more than the energy of Jahn-Teller distortion.<sup>25</sup> *SO* interaction lifts all degeneracies, and the energy shifts are larger than the average level splitting. Spin and orbital quantum numbers are no longer good quantum numbers, and it is difficult to correlate the new orbitals to the symmetries of the undistorted closed-shell case. The energy ladder in Figure 8b is therefore only schematic.

In passing by we note that the filled and the empty shells in Figure 8a have no net spin and are therefore not affected by *SO* coupling. However, it is customary to plot single electron energies, and these levels are therefore also split in Figure 7b. Moreover, in

characterization by optical spectroscopy, an electron from the doubly occupied state is excited to an empty orbital so that both the initial and the final state are affected (compare Figure 7c).

A broad absorption near 2200 cm<sup>-1</sup> (270 meV) was reported for Pt<sub>13</sub> clusters with chemisorbed H/D in the pores of a zeolite.<sup>29</sup> Although it occurs in the infrared, it was assigned to an electronic transition across the HOMO-LUMO gap because of its independence on the mass of the adsorbed hydrogen isotope. The absorption energy is of the order of the average level splitting at 6-8 states per eV. Fully relativistic calculations confirmed a size of the HOMO-LUMO gap of between 30 meV and 190 meV depending on the cluster geometry.<sup>26</sup> Due to the open-shell nature of the clusters, *SO* coupling leads to the situation indicated schematically for the broken symmetry in Figure 8.

For use in discussions of hydrogen-covered Pt<sub>13</sub> clusters further below we have also schematically indicated in Figure 7b the energy of the chemisorbed H atoms. The orbital of the free H atom is at -13.6 eV, much lower than the cluster orbitals near the HOMO-LUMO gap. Each chemisorbed H atom uses one of the cluster electrons for the bond and forms a low-energy hydride-like adduct.

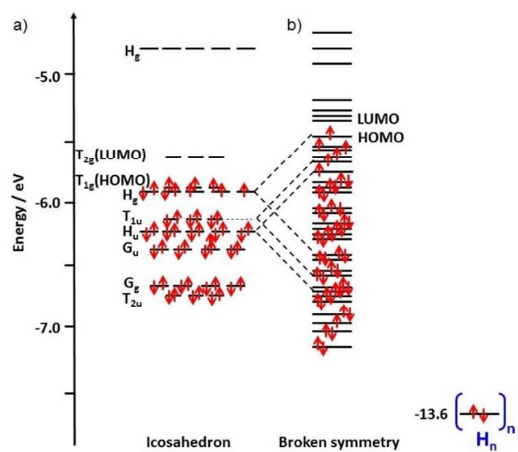


**Figure 8:** a) Calculated valence orbital energy levels of Pt<sub>13</sub> superatom clusters in icosahedral structure, based on data in Ref. 24, and b) schematic presentation in the presence of broken symmetry. The ionization potential of the free H atom is -13.6 eV; cluster chemisorbed H (right) will therefore have significant hydride character. The dashed lines are to indicate qualitatively to what extent the degeneracy of levels is lifted due to *SO* coupling. (Adapted with permission from Ref. 30).

## Evidence from magnetic properties

### Electron spin resonance

**a) Gold:** Magnetic measurements provide additional information about the electronic state since they take into account explicitly the magnetic moments of spin and orbital angular moments as well as their coupling to total angular moments. The most detailed information is available for the thiol-capped gold nanocluster Au<sub>25</sub>(SR)<sub>18</sub>. For the anion we know that it is a closed-shell system

with the HOMO orbital being a triply degenerate singlet P state (Figure 7b). The neutral compound with a hole in the highest orbital is thus  $^3P_{3/2}$ , which is in agreement with Hund's rules for conventional atoms. It is active in electron paramagnetic resonance (EPR) spectroscopy, and its spectrum in frozen solution is given in Figure 9a.<sup>31</sup> It was confirmed by quantitative EPR and SQUID magnetization measurements that there is a single unpaired electron per cluster. The spectrum is highly anisotropic and almost axial, as expected for the electron in a p orbital, with a slight distortion perhaps due to a matrix effect. The isotropic average of the principal  $g$ -components amounts to 2.247, which is considerably larger than  $g_e = 2.0023$ , revealing a significant contribution due to spin-orbit coupling. Thus, the orbital angular momentum is not fully quenched; the unpaired electron must therefore be admixed by a doughnut-shaped p<sub>x</sub> (or p<sub>y</sub>) orbital, other than concluded in ref. 30.  $g > g_e$  is also consistent with the general rule for more than half-filled shells that is well-known for transition metal ions.<sup>32</sup> No hyperfine interaction was resolved, and the fitted hyperfine interactions are approximate, representing the linewidths only. The work was complemented with a careful DFT calculation, confirming that the influence of the gold atoms of the outer shell is negligible. The entire observation is consistent with the superatom picture for the 13-atom core of the compound, and the rules are the same as for conventional atoms.

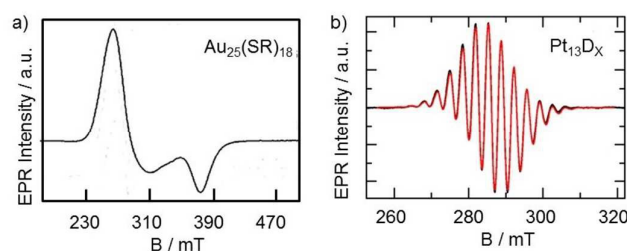


**Figure 9:** a) X-band EPR spectrum of  $\text{Au}_{25}(\text{SR})_{18}^0$  thiol protected nanocluster in frozen  $\text{CH}_2\text{Cl}_2/\text{toluene}$  solution at 7 K. The simulation to this spectrum fits  $\mathbf{g} = (2.556, 2.364, 1.821)$  and  $\mathbf{A} = (71, 142, 50)$  MHz with 13 equivalent  $I = 3/2$  nuclei. (Adapted with permission from Ref. 31. Copyright (2009) by the American Chemical Society). b) Experimental (black line) and simulated (red, nearly indistinguishable) EPR spectra of  $\text{Pt}_{13}\text{D}_x$  clusters at unspecified partial deuterium coverage in zeolite KL recorded at 4 K. This spectrum fits with 12 equivalent Pt nuclei at natural isotopic abundance with  $\mathbf{g} = (2.3795, 2.3615, 2.3615)$  and  $A = 227$  MHz (isotropic). (Adapted with permission from Ref. 19. Copyright (2013) by the American Chemical Society).

**b) Platinum:** As a second superatom-type system,  $\text{Pt}_{13}\text{D}_x$  clusters confined in the pores of zeolites have been investigated in detail by EPR.<sup>19</sup> The spectrum displayed in Figure 9b is split by hyperfine interaction to nuclear spin- $1/2$   $^{195}\text{Pt}$  nuclei which have a natural abundance of 33.8%, all the other nuclei have spin zero. The multiplet is of high quality and can be fit quantitatively assuming 12 equivalent Pt nuclei if their isotropic distribution is taken into account.  $\text{Pt}_{13}\text{H}_x$  clusters show analogous spectra with broader lines, revealing that the hydrogen hyperfine interaction is concealed in the linewidth. The H coupling was resolved in HYSORE experiments.<sup>19</sup> In contrast to the spectrum of the gold cluster in Figure 9a, the spectrum is nearly isotropic with only a small  $g$ -anisotropy, but with a value of 2.3675 the isotropic average of the

$g$ -components is considerably larger than  $g_e$  and reveals significant coupling of the spin to an orbital momentum that is clearly not quenched.

Interestingly, both examples shown in Figure 9 gave  $g$ -values larger than  $g_e$ , while experiments with gold nanoparticles of 5-15 nm diameter gave an average  $g$ -value of  $0.84 \pm 0.39$ , and none of the states had  $g > g_e$ .<sup>24,33,34</sup> It should be noted that gold particles exceeding a diameter of 2.3 nm are metallic,<sup>21</sup> while the ones of Figure 9 are well below this size limit and of molecular nature.

It is significant that the multiplet is due to only 12 coupling Pt nuclei, no coupling is resolved for the central atom of the cluster. This shows that the orbital containing the unpaired electron has a node at the central atom, which is direct evidence for its superatom character. This orbital must be isotropic, but it cannot be of s-character because no spin density is detected at the center. p-type and d-type orbitals do not fulfil the requirement of isotropy. However, for example the f-type orbitals with  $|m| = 2$  have their lobes in the direction to the corners of a cube, and although they are not of spherical symmetry they permit an isotropic spectrum.

#### High-spin clusters: spin and orbital momentum

The spectrum shown in Figure 9b represents <1% of all Pt in the sample and is thus a minority species, likely with one unpaired electron. Before soft desorption of part of the initial chemisorbed hydrogen after preparation a similar but much more anisotropic multiplet is observed. The signal amplitude increases nearly linearly from  $\text{Pt}_{13}\text{D}_6$  to  $\text{Pt}_{13}\text{D}_{30}$ , but it is assumed that a distribution of coverages is present in the samples with the EPR-active species near the high end of the coverage.<sup>19</sup> 10-20% appear to be EPR-silent high-spin clusters, the remaining major fraction of Pt is diamagnetic.<sup>35</sup> The distribution between these species may be influenced by the proximity of exchangeable cations or by water molecules formed during the reduction of PtO with hydrogen. Furthermore, on hydrogen desorption at 573 K the decrease of the Pt-Pt coordination number determined by extended X-ray absorption fine structure spectroscopy (EXAFS) decreases from 5.5(6) to 4.3(6), suggesting restructuring with concomitant lowering of the initial icosahedral or cuboctahedral symmetry.<sup>34</sup> This process is at least partly reversible.

We now focus on the magnetization of high-spin clusters. Central for magnetic moments is the presence of angular moments with non-zero z-component. Unpaired electrons always contribute with their magnetic moment which they can lose only by pairing with another electron. In contrast, the atomic orbital angular momentum is quenched when the symmetry of the free atom is broken. s-orbitals are of spherical symmetry and have z-component zero. Thus, atomic Au with its unpaired electron in a 6s orbital possesses no orbital momentum. The atom in the center of an icosahedral or cuboctahedral 13-atom cluster may contribute atomic angular momentum if there is an unpaired electron with significant non-s orbital population. The symmetry of an atom at the surface of the cluster is also broken, but a rotation axis perpendicular to the surface remains. If there is an unpaired electron with partial occupation of an orbital with such rotational symmetry this may contribute orbital momentum to magnetization, but if all atoms of the cluster contribute then the moments add up to zero.



In superatoms we have to take account of the superatomic (or molecular) orbital momentum in addition to the atomic orbital momentum. Again, the symmetry is crucial, and deviations from rotational symmetry by the environment or when additional atoms are added can reduce or quench completely the contribution to magnetism. More importantly, since this orbital is fixed to the environment of chemical bonds, the orbital momentum is locked to the orientation of the nanoparticle or cluster. These moments are not free to align with an external magnetic field, which has important consequences for the magnetic behavior of nanomaterials. Heterogeneity of particle size and magnetization adds further complications. Nevertheless, hysteresis behavior up to room temperature provides evidence of large magnetic anisotropies related to giant orbital moments (see below).

Experimentally, it was found that the ratio of orbital to spin angular momentum,  $\mu_o/\mu_s$ , equals 0.28(4) for bulk Au and 0.31(6) in 1.9 nm poly(allylamine hydrochloride) capped Au nanoparticles.<sup>7</sup> While bulk gold shows only Pauli paramagnetism, the nanoparticles are ferromagnetically polarized, and their large magnetization was ascribed to a contribution of orbital momentum by spin-orbit coupling.<sup>7</sup>

Detailed information is available for monodisperse Pt nanoclusters with  $13 \pm 2$  atoms, as determined from EXAFS.<sup>19,36</sup> Up to 3 H atoms per surface atom can be bound in a configuration in which they bridge the Pt–Pt bonds.<sup>29,35</sup>

The effective magnetic moment per cluster in zeolite L was determined from SQUID measurements after correction for the magnetization of the empty zeolite by fitting the temperature dependence of the magnetization obtained to the Curie law. The values displayed in Table 1 reveal values between 2.5 and 3.4  $\mu_B$ , depending on coverage of the cluster with H, and some equilibrating evolution with time. This coverage dependence is understood based on Figure 8. Each hydrogen atom pairs with one of the electrons from the highest occupied cluster orbital so that the number of unpaired electrons can be “titrated”, letting it go to zero and then increasing it when the electrons are taken from the next lower orbital. The values in Table 1 confirm such an oscillation, although the magnetization does not go to zero, which is explained by the fact that the samples contain a distribution of cluster species  $Pt_{13}H_x$  with various values of  $x$ . Earlier measurements with the same cluster in zeolite NaY but less well defined hydrogen coverage gave values of  $\mu_{eff}$  as high as  $8.4(6)\mu_B$ .<sup>36</sup> The ratio of orbital-to-spin contribution was found from XMCD to be  $\mu_o/\mu_s = 0.30(2)$ , or 23%, 0.29(2) for  $Pt_{13}H_x$ , significantly less than the value of 0.38(2) for bulk Pt foil.<sup>8</sup> The values of  $\mu_o/\mu_s$  which are the largest ever found for a Pt compound were confirmed by fully relativistic calculations of the  $Pt_{13}$  cluster in various geometries.<sup>26</sup> It should be noted that XMCD excites an intra-atomic transition and is therefore sensitive to the atomic but not the superatomic orbital angular momentum. Since the relativistic calculations could reproduce the experimental values of  $\mu_o/\mu_s$  but not the large values of  $\mu_{eff}$  this may be taken as an indication that the superatomic orbital momentum indeed plays an important role.

Table 1: Magnetization  $\mu_{eff}$  for high-spin  $Pt_{13}H_x$  clusters in zeolite KL<sup>19</sup>

H coverage x	12(2)	18(2)	23(2)	29(2)	38(2)
$\mu_{eff}/\mu_B$ per cluster	3.4(2)	2.5(2)	2.8(2)	3.0(2)	2.9(2)
		2.9(2)*			3.1(2)*

\*Same sample measured 2 months later

### Giant magnetic anisotropy

It is meanwhile well accepted and understood that metals like gold or platinum become magnetic if present in nanosize dimensions. It is, however, extremely intriguing that such magnetism of spherical gold nanoparticles as small as 1.4 nm (corresponding to 85 Au atoms in the average) shows hysteresis similar to long-range ordered ferromagnetic matter, and even more that hysteresis may be observed up to room temperature (Figure 10a) and beyond.<sup>37</sup> The observation of a splitting or blocking temperature  $T_b$  is typical for single domain superparamagnetic nanoparticles which undergo a transition to a blocked state where the Néel relaxation time of magnetization  $\tau_N$  becomes slow compared to the time scale  $\tau_m$  of a particular method of measurement. Below  $T_b$  the magnetization is frozen and depends on the magnetic field during cooling. The Néel relaxation is activated because of the nanoparticle’s magnetic anisotropy and given by the relation:<sup>38</sup>

$$\tau_N = \tau_0 \exp\left(\frac{KV}{k_B T}\right), \quad (1)$$

where  $\tau_0$  is the Arrhenius pre-exponential factor, typically  $10^{-9} - 10^{-10}$  s. For a conventional magnetic material, the magnetization is blocked when the anisotropy energy barrier  $E_A = K \cdot V$  is of the order of  $k_B T$ , with  $K$  the anisotropy energy,  $V$  the volume and  $k_B$  the Boltzmann constant.<sup>6</sup> A 1.4 nm nanoparticle exhibiting a stable magnetization at 300 K should therefore possess an anisotropy energy  $K$  in excess of  $2.4 \times 10^8$  J m<sup>-3</sup>, approximately 26 meV for each of the 85 gold atoms, which is enormous. This is to be compared with 1.2 meV per Co atom for hexagonal  $SmCo_5$ , a strong classical magnetic material.<sup>37</sup>

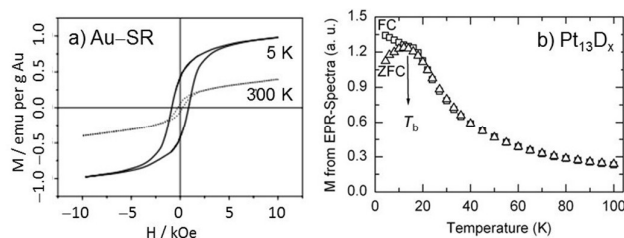
Magnetic nanomaterials consist typically of single domain particles with behavior different from ferromagnetism which is a long-range ordered state. They are superparamagnetic, reminding of paramagnetism of a superspin, but below a blocking temperature a hysteresis loop may open up. The loops reported in Figure 10a are typical for heterogeneous nanomaterials in several respect.<sup>39</sup> The hysteresis loops persist up to room temperature, revealing large magnetic anisotropy as discussed above, but the loop at 300 K is considerably smaller than the one at 5 K. This shows that only a fraction of the particles is blocked up to 300 K, the others experience a lower anisotropy energy barrier  $E_A$ . Secondly, the sample is not saturated at any temperature, revealing incomplete alignment of the magnetic moments at 10 kOe ( $\approx 1$  T). The saturation curve at 300 K probably never reaches the one at 5 K, indicating that the total moment decreases with temperature due to spin pairing or reduction of the orbital moment. The lower slope of the loop at the intersection with the field axis confirms that the average moment of the individual particles is lower at 300 K.

Figure 10b shows the temperature dependence of the integrated intensity of the EPR multiplet (Figure 9b) of a  $Pt_{13}D_x$  sample in Pt/KL zeolite at intermediate deuterium coverage. Interestingly, the

magnetization curves following cooling in zero field (ZFC) and in the EPR field (FC at *ca.* 0.290 T) split below  $T_b = 14$  K. The X-band EPR frequency in the present experiment corresponds to  $10^{-10}$  s. At the blocking temperature,  $T = T_b$ ,  $\tau_N$  in eqn. (1) is set equal to  $\tau_m$ , so that

$$\tau_m = \tau_0 \exp\left(\frac{KV}{k_B T_b}\right),$$

or:  $KV = k_B T_b \ln(\tau_m / \tau_0)$ . (2)



**Figure 10:** a) Hysteresis loops obtained with thiol-capped 1.4 nm Au nanoparticle at 5 K and 300 K (reprinted with permission from Ref. 37. Copyright (2004) by the American Physical Society). b) Magnetization derived from the intensity of the multiplet of EPR-active  $\text{Pt}_{13}\text{D}_x$  in iron-free KL zeolite after gentle deuterium desorption. EPR measurements are on increasing temperature following zero-field cooling (ZFC) and field cooling (FC at 290 mT) to 4.5 K (Reproduced with permission from Ref. 30).

For typical laboratory experiments,  $\ln(\tau_m/\tau_0)$  is on the order of 25.<sup>40</sup> For the observed blocking temperature,  $T_b = 14$  K, we obtain an activation barrier  $K \cdot V$  of 0.30 eV (23 meV per Pt atom, coinciding with the 26 meV per gold atom derived from the hysteresis behavior for the Au nanoparticle). 0.30 eV is of the same order as the spin pairing interaction mentioned previously and the average splitting of energy levels with 6–8 states per eV near the Fermi energy.

The observation of Figure 10b is intriguing since the EPR active species represents a minority species (<1% of the total Pt in the sample), and yet the blocking temperature of 14 K is within small variations dependent on D coverage the same as that observed by bulk SQUID magnetization measurements<sup>19</sup> which represent mostly the EPR-silent high-spin fraction (10-20%). The loading with Pt (6 wt.%) is sufficiently small that there is no magnetic interaction between the clusters. The EPR spectrum reflects the population difference between electron spin  $\alpha$  and electron spin  $\beta$  states and scales normally as  $1/T$  (Curie behavior). Except for its amplitude, plotted in Figure 10b, it is entirely independent of temperature, including its position on the magnetic field axis. The EPR-active species acts as a local spectator, but it provides no evidence that the local magnetic field is any different at low temperature. Thus, we must conclude that during cooling to 4 K in zero field about 1/6 of the clusters are transformed and locked in an EPR-silent form, while cooling in the applied field keeps them in their active form. It must have to do with a field-induced shift of energy levels. An electron spin can contribute only  $0.29 \text{ T} \times \mu_B = 0.017 \text{ meV}$  at this field. We need a factor 180 more, and a large orbital momentum as inferred above for small gold nanoparticles may be able to do the trick.

The cluster with nominal saturation hydrogen coverage,  $\text{Pt}_{13}\text{H}_{38}$ , was the only one among five coverages that showed plain Curie behavior without a  $\chi_D$  maximum that would indicate blocking.<sup>19</sup> Based on the above reasoning this state must be one with the unpaired electron in an orbital with  $L_z = 0$ . This could also be the state that is EPR-active.

A candidate for interesting magnetic effects is the intrinsically chiral gold nanocluster  $[\text{Au}_{20}(\text{PP}_3)_4]^{4+}$  with  $(\text{PP}_3)_4 = \text{tris}(2\text{-}(diphenylphosphino)\text{-ethyl})phosphine$  (Figure 11). Magnetic measurements have not yet been reported, but the electronic ground state was predicted to be of approximate  $^3D$  symmetry, i.e. a triplet state with two electrons in a superatom orbital with  $L = 2$ , and with a 1.3 eV gap to the first LUMO state.<sup>41</sup> The orbital moment is expected to be locked to the rigid enantiomeric structure, and if Hund's third rule applies, the antiparallel coupling of orbital and spin momentum is energetically favored (Figure 11b). However, in the presence of an external magnetic field there will be a complex competition between the aligning force of the orbital momentum and the external field for the orientation of the electron spin. One should expect a hysteresis loop akin to that shown in Figure 10a, but this system is much better defined, which should permit quantitative simulation. The recently reported enantioseparation will further ease the interpretation,<sup>42</sup> it would be of particular interest to analyze the chirality-dependent interaction with the magnetic field.

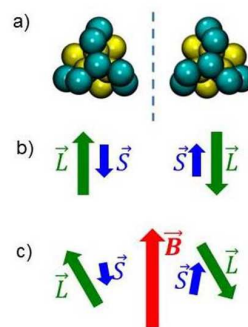


**Figure 11:** a) Top view of the two enantiomers of the intrinsically chiral  $[\text{Au}_{20}(\text{PP}_3)_4]^{4+}$  nanocluster with the 13-atom icosahedral core (yellow) and the chiral 7-atom triblade clamp (blue). The  $\text{PP}_3$  capping ligands which are non-chiral as free molecules are omitted for clarity.<sup>41</sup> b) Side view of the orientation of the superatom orbital angular momentum  $\vec{L}$  and the spin angular momentum  $\vec{S}$  assumed antiparallel to  $\vec{L}$  in the absence of an external magnetic field. c) Schematic view of the magnetic moments in the presence of a magnetic field  $\vec{B}$ .  $\vec{L}$  is locked to the orientation of the cluster, while  $\vec{S}$  aligns with the effective field of  $\vec{L}$  and  $\vec{B}$ , and with increasing  $\vec{B}$  the electron spins might flip their orientation.

#### Anomalous diamagnetic susceptibility

Interestingly, the high-spin paramagnetic magnetization that dominates the picture at low temperature disappears relatively quickly, and at room temperature only linear behavior as a function of magnetic field is observed with a negative slope, revealing a pronounced diamagnetism, as shown in Figure 12. The magnetic susceptibility  $\chi_D$  depends again on hydrogen coverage and is a

factor 36-50 higher than tabulated values for diamagnetic Pt.<sup>43</sup> This behavior of superdiamagnetism had been predicted for sodium clusters.<sup>44</sup> The explanation is based on the assumption that circular currents exist on the superatom instead of on the individual atoms. The magnetic moment scales with the square of the radius of the circular current. While the picture is qualitatively correct it falls short in reproducing the effect quantitatively if only the Pt atoms are included in a simple classical simulation. Furthermore, diamagnetism is larger for Pt<sub>13</sub>H<sub>38</sub> than for Pt<sub>13</sub>H<sub>18</sub>, revealing again a contribution of the shell of chemisorbed hydrogen. Including the hydride shell in the simulation leads to a satisfactory agreement with experiment.<sup>43</sup> Note that for the given 13-atom nanocluster,  $\chi_D$  is negative and predicted to increase in magnitude with cluster size. However, bulk Pt exhibits temperature-dependent  $\chi_D > 0$ , which requires a reversal of the behavior and a change of sign for larger particles.<sup>45</sup> It would therefore be of interest to map out the size dependence.

Similar behavior was reported for 2.2 nm and 3.5 nm Au nanoparticles without further comment<sup>6</sup> and for Cu<sub>9</sub> nanoclusters.<sup>46</sup> It should be interesting to investigate also the well characterized atomically precise gold clusters that are available today.<sup>10</sup>

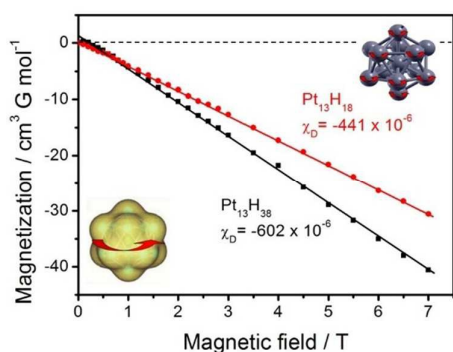


**Figure 12:** SQUID results of magnetization at 300 K of Pt<sub>13</sub>H<sub>18</sub> (red) and Pt<sub>13</sub>H<sub>38</sub> (black) supported in specifically synthesized iron-free KL zeolite after correction for the magnetization of the empty zeolite (symbols and full lines) compared with calculated curves (broken lines and numbers in parentheses). The numbers relate to one mol of Pt atoms with  $\chi_D$  in units of cm<sup>3</sup>·mol<sup>-1</sup>. The inset shows the classical model to explain diamagnetism based on induced ring currents on the atom and on the superatom. (Adapted with permission from ref. 30).

## The chemistry of superatoms

Key work in the group of Welford Castleman was centered on aluminum clusters.<sup>5</sup> Atomic Al has three valence electrons and is a typical metal with an electron affinity of 0.43 eV. Al<sub>13</sub> has 39 valence electrons, which it would like to fill up to the noble-gas-like closed shell of 40 electrons (Figure 4). Its electron affinity is 3.34 eV, nearly 8 times that of atomic Al; it is thus a halogen-like superatom comparable to chlorine, with EA = 3.6 eV. As we learned from Figures 5b and 6, EA increases with the number of atoms in the cluster due to the evolution towards a band structure. Theoretical calculations for Al<sub>13</sub><sup>-</sup> found the negative charge on the metal

cluster while the iodine atom remains nearly neutral. This illustrates impressively the distinct and surprising properties that superatoms can have.<sup>47-50</sup>

The increase of EA and simultaneous decrease of IP are at the cost of the HOMO-LUMO gap (or the band gap in semiconductors), which is often taken as an indicator of stability of molecular species. This general criterion rests on the fact that at a large gap the high IP and low EA make the species difficult to oxidize as well as to reduce, and also covalent bonds are stronger when the energies of orbitals engaged in bonding are of comparable magnitude. For Al<sub>13</sub>, the gap still amounts to 1.8 eV, underlining its stability that is confirmed also by the calculated cohesive energy of 2.58 eV per atom. In general, one should be aware that larger superatoms tend to be more reactive.<sup>5</sup>

One may question the usefulness of the concept of superatoms as building blocks in chemistry. To be useful they must be energetically sufficiently stable, chemically inert and allow the formation of defined chemical entities by forming bonds to other atoms. If we consider ligand-protected *nanoparticles* then we talk about an entity in which neither the number of atoms in the core nor the number of ligands is accurately known. However, a number of ligand-protected *nanoclusters* with well-defined stoichiometry and structure are known. Figure 12 shows the example of Au<sub>25</sub>(SR)<sub>18</sub>, or equivalently Au<sub>13</sub>[R-S(AuSR)<sub>2</sub>], that was discussed also in Figure 8a. It is a stable and well-defined species that can be reduced reversibly to its anion.<sup>31</sup> The superatom core can be doped by replacing one of the Au atoms by a different element, e.g. Cu, Hg, Ag, Pt, Cd, or Pd.<sup>51</sup>

The system of Figure 13 reminds of metalorganic chemistry, which is a well-established and prominent field of chemistry. It describes compounds in which various ligands coordinate to a central atom or ion, often a transition metal in various charge states, and their spectroscopy, electrochemistry and even catalytic activity are well known. It is imagined that the transition metal is replaced by a superatom and the ligands adapted to the larger core and its different electronic properties. Considering the creativity of the chemical community this will initiate an entirely new branch of chemistry with many new degrees of freedom to be explored.

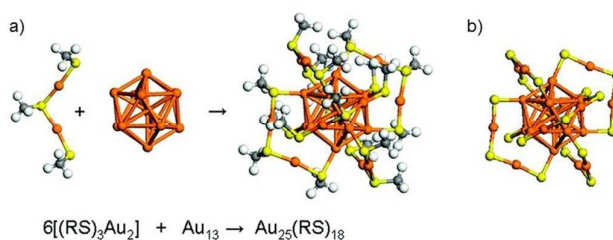


**Figure 13:** a) Complexation reaction of a central icosahedral Au<sub>13</sub> superatom with six R-S(AuSR)<sub>2</sub> bidentate ligands to give Au<sub>25</sub>(SR)<sub>18</sub> or Au<sub>13</sub>[R-S(AuSR)<sub>2</sub>]<sub>6</sub>. R can be H or alkyl (here CH<sub>3</sub>). b) For clarity, the structure of the complex is shown under omission of R. Each ligand acts as a 'staple' when it binds to two next-nearest neighbors of the 12 superatom sulfurs, giving an overall octahedral arrangement. (Reprinted with permission from Ref. 52. Copyright (2008) by the American Chemical Society).

Most current electrolytes in Li-ion batteries such as LiAsF<sub>6</sub>, LiBF<sub>4</sub>, LiPF<sub>6</sub>, LiFePO<sub>4</sub>, LiClO<sub>4</sub>, LiN(SO<sub>2</sub>F)<sub>2</sub> and LiN(SO<sub>2</sub>CF<sub>3</sub>)<sub>2</sub> contain halogens,

either F or Cl, which are toxic and also corrosive. One of the goals in energy applications is to find halogen-free alternatives without compromising battery performance.<sup>53</sup> The availability of superhalogens like  $\text{BH}_4^-$  (closed shell of  $3 + 4 + 1 = 8$  electrons),  $\text{BO}_2^-$  (EA of  $\text{BO}_2 = 4.3$  eV, 8 electrons, isoelectronic with  $\text{CO}_2$ ), the *closo*-borane cluster  $\text{B}_{12}\text{H}_{12}^{2-}$  (closed shell of  $12 \times 3 + 12 + 2 = 50$  electrons, a dianion that is stable in the gas phase),  $\text{CB}_{11}\text{H}_{12}^-$  (50 electrons, EA of  $\text{CB}_{11}\text{H}_{12} = 5.39$  eV) and others extends considerably the available options to design a tailored material. It was indeed found that a  $\text{CB}_{11}\text{H}_{12}$ -based electrolyte exhibited “unparalleled lithium and sodium superionic conduction in solid electrolytes ( $>0.1$  S  $\text{cm}^{-1}$ )... unmatched by any other known polycrystalline materials at this temperature”.<sup>54</sup>

A similar situation exists for solar cells where the alignment of the band edges between donor, acceptor and electrode components plays an essential role. The new shooting star in photovoltaics are perovskite-based solar cells, with energy efficiencies that have reached values exceeding 22% in late 2017, which makes them close to competitive with conventional silicon or other solid state semiconductor cells, and this after a development time of less than a decade. There are still problems, though, with stability, related to sensitivity against moisture, and ironically also to intense light. The most commonly studied perovskite absorber,  $\text{ABX}_3$ , consists of the organic cation  $\text{A} = \text{CH}_3\text{NH}_3^+$ , the inorganic cation  $\text{Pb}^{2+}$  (or  $\text{Sn}^{2+}$ , but with lower efficiency), and a halogenide  $\text{X}^- = \text{I}^-$ ,  $\text{Br}^-$ , or  $\text{Cl}^-$ . The optical bandgap can be tuned between 1.5 and 2.2 eV by changing the halide content. One would like to have environmentally friendlier alternatives for the halide, and also for lead, which is even more of a concern. Again, the superhalides offer additional degrees of freedom as regards ion diameter and electron affinity. Both properties affect the band gap, which decreases with increasing halide radius and increases with higher bond ionicity, defined as the electronegativity difference between anion and cation.<sup>53</sup> Because of their enhanced stability, superatoms may be chemically more inert.<sup>55</sup>

Many more options of superatom chemistry have been outlined in an authoritative recent review.<sup>53</sup>

## Conclusions

The concept that near-spherical metal clusters with a countable number of member atoms mimic the properties of conventional atoms. The similarity of the angular dependence of their orbitals with hydrogen-like orbitals offers a convincing way of understanding their behavior. Such clusters are therefore called “superatoms”. The consequences of electronic shells that are the basis for the periodic table are familiar to every chemist. Therefore, finding a similar shell structure as a function of cluster size, it appears logical and inspiring to add cluster size as a third dimension to the periodic table.

It is straightforward to understand that clusters with closed electronic shells possess a particular noble gas-like stability, but it may be more useful to find clusters with an electron affinity that surpasses that of halogen atoms. If they are built from cheap, abundant, non-toxic and non-corrosive elements they can be considered as substitutes of halides in batteries or in solar cells. This provides additional options for the design of novel materials in

energy applications where the matching of band gaps and band edges by tuning cluster size is particularly essential for their energy efficiency and stability.

Ligands can stabilize clusters of various charges in the same way as we know it from transition metal complexes, but again we gain a new degree of freedom to discover novel chemistry with as yet unforeseen consequences.

Ionization potential and electron affinity can be tuned by several eV as a function of cluster size. This represents the most important size-effect with marked implications on their catalytic activity and on applications for solar cells and energy storage materials.

To be useful, superatoms should have a certain stability, a property that according to a well-known principle in chemistry is directly related to the size of the HOMO-LUMO or band gap. This gap decreases with cluster size and disappears at the transition to metallic behavior. It places an upper limit on the size of clusters that are sufficiently stable and therefore useful for practical applications.

Relatively little attention has been paid so far on the magnetic behavior of clusters consisting of elements which are not magnetic in the bulk. The number of unpaired electrons matters. Therefore, the number of atoms in the cluster and the influence of nature and coverage dependence of capping ligands must be exactly known. For nanoparticles which are not atomically precise this is not the case, and this has led to confusing and seemingly contradictory reports on the magnetism of noble metal clusters.

Furthermore, the fact that open-shell superatoms in environments of spherical or cylindrical symmetry possess a cluster orbital momentum which may contribute significantly to magnetic behavior has been almost entirely overlooked. The orientation of this magnetic moment is locked to its environment, and this can lead to extremely large magnetic anisotropy and to hysteresis behavior up to room temperature. This could lead to interesting applications in future information technology. However, just as the atomic orbital moment in bonded situations, the superatomic orbital moment is quenched to a large extent if symmetry is sufficiently distorted by the environment or by adding atoms to closed shell configurations.

More work needs to be done on some fundamental aspects of superatoms. For example, their spectroscopy is not well known. Selection rules based on the extent of symmetry can assist in the assignment of transitions. XMCD is based on an intra-atomic transition that provides a measure of *atomic* angular momentum. A method that probes the analogous *superatomic* momentum would be highly desirable. Spin-orbit coupling to orbital moments need to be clarified and the coupling coefficients calculated. Also the implications of the extraordinary diamagnetism of metal clusters needs further theoretical work.

## Conflicts of interest

There are no conflicts to declare.

## Notes and references

1. S. N. Khanna, P. Jena, Atomic clusters: building blocks for a class of solids", *Phys. Rev. B*, 1995, **51**, 13705–13717.
2. S. N. Khanna, P. Jena, *Chem. Phys. Lett.*, 1994, **219**, 479–483.
3. G. I. Nierenberg. "The art of creative thinking", Simon & Schuster, New York, (1986) p. 201.
4. P. Ball, A new kind of alchemy, *New Scientist*, 13 April 2005.
5. A. W. Castleman Jr., S. N. Khanna, Clusters, superatoms, and building blocks of new materials, *J. Phys. Chem. C*, 2009, **113**, 2664–2675.
6. G. L. Nealon, B. Donnio, R. Greget, J.-P. Kappler, E. Terazzi, J. L. Gallani, Magnetism in gold nanoparticles, *Nanoscale*, 2012, **4**, 5244–5258.
7. M. Suzuki, N. Kawamura, H. Miyagawa, J. S. Garitaonandia, Y. Yamamoto, H. Hori, Measurement of Pauli and orbital paramagnetic state in bulk gold using X-ray magnetic circular dichroism spectroscopy, *Phys. Rev. Lett.* 2012, **108**, 047201.
8. J. Bartolomé F. Bartolomé, L. M. García, E. Roduner, Y. Akdogan, F. Wilhelm, A. Rogalev, Magnetization of Pt<sub>13</sub> clusters supported in NaY zeolite: a XANES and XMCD study. *Phys. Rev. B*, 2009, **80**, 014404.
9. M. Niemayer *et al.* Spin coupling and orbital angular momentum quenching of free iron clusters, *Phys. Rev. Lett.*, 2012, **108**, 057201.
10. S. Knoppe, T. Bürgi, Chirality in thiolate-protected gold clusters, *Acc. Chem. Res.*, 2014, **47**, 1318–1326.
11. T. P. Martin, Shells of atoms; *Physics Reports*, 1996, **273**, 199–242.
12. W. A. de Heer, The physics of simple metal clusters: Experimental aspects and simple models; *Rev. Mod. Phys.* 1993, **65**, 611–676.
13. R. G. Polozkov, V. K. Ivanov, A. V. Verkhovtsev, A. V. Korol, A. V. Solov'yov, New applications of the jellium model for the study of atomic clusters, *J. Phys., Conf. Ser.*, 2013, **438**, 012009.
14. S. Neukermans, E. Janssens, Z. F. Chen, R. E. Silverans, P. v. R. Schleyer, P. Lievens, Extremely stable metal-encapsulated AlPb<sub>10</sub><sup>+</sup> and AlPb<sub>12</sub><sup>+</sup> Clusters: Mass-Spectrometric Discovery and Density Functional Theory Study, *Phys. Rev. Lett.* 2004, **92**, 163401.
15. E. Janssens, S. Neukermans, P. Lievens, Shells of electrons in metal-doped simple metal clusters, *Current Opinion in Solid State & Materials Science*, 2004, **8**, 185–193.
16. D. Jiang, M. Kühn, Q. Tang, F. Weigend, Superatomic orbitals under spin-orbit coupling, *J. Phys. Chem. Lett.*, 2014, **5**, 3286–3289.
17. E. Roduner, *Nanomaterials – Size-dependent phenomena and growth principles*, 2<sup>nd</sup> Ed., Royal Society of Chemistry, Cambridge, 2014.
18. H. Häkkinen, Atomic and electronic structure of gold structures: understanding flakes, cages and superatoms from simple concepts, *Chem. Soc. Rev.*, 2008, **37**, 1847–1859.
19. C. Jensen, J. van Slageren, P. Jakes, R.-A. Eichel, E. Roduner, Support effects on hydrogen desorption, isotope exchange, chemical reactivity, and magnetism of platinum nanoclusters in KL zeolite. *J. Phys. Chem. B*, 2013, **117**, 22732–22745.
20. K. J. Taylor, C. L. Pettiette-Hall, O. Cheshnovsky, R. E. Smalley. *J. Chem. Phys.* 1992, **96**, 3319–3329.
21. J. Zheng, C. Zhang, R. M. Dickson, Highly fluorescent, water-soluble, size-tunable gold quantum dots, *Phys. Rev. Lett.*, 2004, **93**, 077402.
22. M. Zhou, C. Zeng, Y. Chen, S. Zhao, M. Y. Sfeir, M. Zhu, R. Jin, Evolution from the plasmon to exciton state in ligand-protected atomically precise gold nanoparticles, *Nature Comm.*, 2016, **7**, 13240.
23. N. E. Christensen, Spin-orbit projected d-densities of states of Pd, Ag, Pt, Au. *J. Phys. F: Met. Phys.*, 1978, **8**, L51–L55.
24. F. Kuemmeth, *Spin states and spin-orbit coupling in nanostructures*, PhD thesis, Cornell University, 2008.
25. N. Watari, S. Ohnishi, Atomic and Electronic Structures of Pd<sub>13</sub> and Pt<sub>13</sub> Clusters. *Phys. Rev. B Condens. Matter*, 1998, **58**, 1665–1677.
26. O. Bunău, J. Bartolomé, F. Bartolomé, L. M. García, Large orbital magnetic moment in Pt<sub>13</sub> clusters, *J. Phys.: Condens. Matter*, 2014, **26**, 19600.
27. X. Liu, H. Dilger, R.-A. Eichel, J. Kunstmann, E. Roduner, A small paramagnetic platinum cluster in a NaY zeolite: characterization and hydrogen adsorption and desorption. *J. Phys. Chem. B* 2006, **110**, 2013–2023.
28. L. G. Vanquickenborne, L. Haspeslagh, On the meaning of the spin-pairing energy in transition-metal ions. *Inorg. Chem.*, 1982, **21**, 2448–2454.
29. M. Keppeler, E. Roduner, Platinum-hydrogen vibrations and low energy electronic transitions in 13-atom Pt nanoclusters, *Phys. Chem. Chem. Phys.*, 2014, **16**, 26613–26616.
30. E. Roduner, C. Jensen, Magnetic properties and the superatom character of platinum nanoclusters, *Magnetochemistry*, 2015, **1**, 28–44.
31. M. Zhu, C. M. Aikens, M. P. Hendrich, R. Gupta, H. Qian, G. C. Schatz, R. Jin, Reversible switching of magnetism in thiolate-protected Au<sub>25</sub> superatoms, *J. Amer. Chem. Soc.*, 2009, **131**, 2490–2492.
32. K. Dyrek, M. Che, EPR as a tool to investigate the transition metal chemistry on oxide surfaces, *Chem. Rev.*, 1997, **97**, 305–331.
33. F. Kuemmeth, K. I. Bolotin, S.-F. Shi, D. C. Ralph, Measurement of discrete energy level spectra in individual chemically synthesized gold nanoparticles, *Nano Lett.*, 2008, **8**, 4506–4512.
34. J. von Delft, D. C. Ralph, Spectroscopy of discrete energy levels in ultrasmall metallic grains, *Phys. Rep.*, 2001, **345**, 61–173.
35. C. Jensen, D. Buck, H. Dilger, M. Bauer, F. Philipp, E. Roduner, Maximum hydrogen chemisorption on KL zeolite supported Pt clusters. *Chem. Commun.*, 2013, **49**, 588–590.
36. X. Liu, M. Bauer, H. Bertagnolli, E. Roduner, J. van Slageren, F. Philipp, Structure and magnetization of small monodisperse platinum clusters. *Phys. Rev. Lett.*, 2006, **97**, 253401; 2009, **102**, 049902E.
37. P. Crespo, R. Litrán, T. C. Rojas, M. Multigner, J. M. de la Fuente, J. C. Sánchez-López, M. A. García, A. Hernando, S. Penadés, A. Fernández, Permanent magnetism, magnetic anisotropy, and hysteresis of thiol-capped gold nanoparticles, *Phys. Rev. Lett.*, 2004, **93**, 087204.
38. I. D. Zhang, J. D. Budnick, W. A. Hynes, C. L. Chien, J. Q. Xiao, Effect of the magnetic field on the superparamagnetic relaxation in granular Co-Ag samples. *Appl. Phys. Lett.*, 1998, **72**, 2053–2055.
39. E. C. Stoner, E. P. Wohlfarth, A Mechanism of magnetic hysteresis in heterogeneous alloys, *Trans. Roy. Soc.*, 1948, **A240**, 599–642.

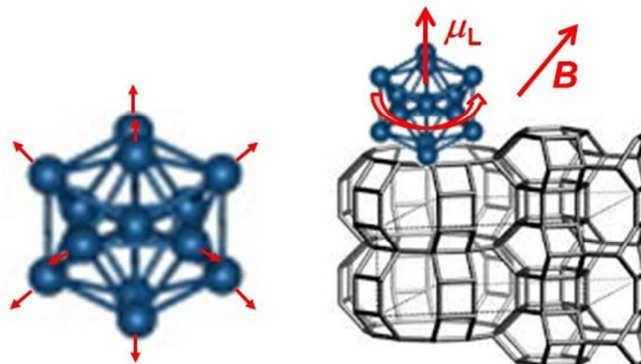
40. J. B. Hickey, M. A. Howson, D. Greig, N. Wiser, Enhanced magnetic anisotropy energy density for superparamagnetic samples of cobalt. *Phys. Rev. B*, 1996, **53**, 32–33.
41. S. Knoppe, L. Lehtovara, H. Häkkinen, Electronic structure and optical properties of the intrinsically chiral 16-electron superatom complex  $[\text{Au}_{20}(\text{PP}_3)_4]^{4+}$ , *J. Phys. Chem. A*, 2014, **118**, 4214–4221.
42. Y. Zhu, H. Wang, K. Wan, J. Guo, Ch. He, Y. Yu, L. Zhao, Y. Zhang, J. Lv, L. Shi, R. Jin, X. Zhang, X. Shi, Z. Tang, Enantioseparation of  $[\text{Au}_{20}(\text{PP}_3)_4]^{4+}\text{C}_{60}$  clusters with intrinsically chiral cores, *Angew. Chem. Int. Ed.*, 2018, **57**, 9059–9063.
43. E. Roduner, C. Jensen, J. van Slageren, R. A. Rakoczy, O. Larlus, M. Hunger, Anomalous diamagnetic susceptibility in 13-atom platinum nanocluster superatoms, *Angew. Chem. Int. Ed.*, 2014, **53**, 4318–4321.
44. V. Kresin, Electronic structure of small metal clusters: Thomas-Fermi statistical theory, *Phys. Rev. B*, 1988, **38**, 3741–3746.
45. A. Schindler, R. König, T. Herrmannsdörfer, H. F. Braun, G. Eska, D. Günther, M. Meissner, M. Mertig, R. Wahl, W. Pompe, Superconductivity at 20 mK in compacted submicrometer platinum powders, *Physica B*, 2003, **329-333**, 1427–1428.
46. Y. Raju, P. Krishnamurthi, P. L. Paulose, P. T. Manoharan, Substrate-free copper nanoclusters exhibit super diamagnetism and surface based soft ferromagnetism, *Nanoscale*, 2017, **9**, 17963–17963.
47. D. E. Bergeron, A. W. Castleman, Jr., T. Morisato, S. N. Khanna, Formation of  $\text{Al}_{13}\text{F}^-$ : Evidence for the superhalogen character of  $\text{Al}_{13}$ , *Science*, 2004, **304**, 84–87.
48. S. J. Peppernick, K. D. Dasitha Gunaratne, A. W. Castleman, Jr., Superatom spectroscopy and the electronic state correlation between elements and isoelectronic counterparts, *PNAS*, 2010, **107**, 975–980.
49. S. J. Peppernick, K. D. Dasitha Gunaratne, A. W. Castleman, Jr. Towards comprehending the superatomic state of matter, *Chem. Phys. Lett.*, **489**, 1–11 (2010).
50. A. W. Castleman, Jr., From elements to clusters: The periodic table revisited, *J. Phys. Chem. Lett.*, 2011, **2**, 1062–1069.
51. M. Zhou, C. Yao, M. Y. Sfeir, T. Higaki, Z. Wu, R. Jin, Excited-state behaviors of  $\text{M}_1\text{Au}_{24}(\text{SR})_{18}$  nanoclusters: the number of valence electrons matters, *J. Phys. Chem. C*, 2018, **122**, 13435–13442.
52. J. Akola, M. Walter, R. L. Whetten, H. Häkkinen, H. Grönbeck, On the structure of thiolate-protected  $\text{Au}_{25}$ . *J. Amer. Chem. Soc.*, 2008, **130**, 3756–3757.
53. P. Jena, Q. Sun, Superatomic clusters: design rules and potential for building blocks of materials, *Chem. Rev.*, 2018, **118**, 5755–5870.
54. W. S. Tang, A. Unemoto, W. Zhou, V. Stavila, M. Matsuo, H. Wu, S.-I. Orimo, T. J. Udovic, Unparalleled lithium and sodium superionic conduction in solid electrolytes with large monovalent cage-like anions. *Energy Environ. Sci.*, 2015, **8**, 3637–3645.
55. A. C. Reber, S. N. Khanna, Superatoms: electronic and geometric effects on reactivity, *Acc. Chem. Res.*, 2017, **50**, 255–263.

**Graphical abstract**

Superatom Chemistry:

Promising Properties of Near-Spherical Noble Metal Clusters

Emil Roduner



Atomic angular moments are nearly quenched in bonded structures, but superatoms in cylindrical environments develop molecular orbital moments.